Effect of Wake Meandering on Aeroelastic Response of a Wind Turbine Placed in a Park

IOP Conf. Series: Journal of Physics: Conf. Series **1356** (2019) 012039 doi:10.1088/1742-6596/1356/1/012039

Effect of Wake Meandering on Aeroelastic Response of a Wind Turbine Placed in a Park

B Panjwani[1], M Kvittem[2], L Eliassen[2], and H Ormberg[2], M Godvik[3]
[1]SINTEF Industry ASA, Trondheim, Norway
[2]SINTEF Ocean ASA, Trondheim, Norway
[3]Equinor ASA, Bergen, Norway

Abstract. A wind turbine operating inside a wind farm is subjected to increased turbulence intensity and reduced wind speeds resulting in increased fatigue loadings and reduced power production. Furthermore, meandering of the wakes results in increased dynamic loading of the wind turbine. In the present study, a standalone dynamic wake meandering (DWM) model has been developed and implemented in commercial code SIMA. The standalone DIWA model does not require a direct coupling with aeroelastic code, hence it is computationally fast. Although the standalone tool is a good alternative for power and thrust prediction, it does not have the capability to predict the turbine aeroelastic loads. The new DWM program is referred as "Disturbed Inflow Wind Analyzer" (DIWA). Benchmarking studies of DIWA with the literature data are presented and discussed. Overall the DIWA compares well with the literature data and the discrepancies between DIWA and the literature data are discussed. The present studies show that the wake deficit profiles are very sensitive to the eddy viscosity parameters. Finally, the turbulence boxes generated using DIWA have been used for understanding the aeroelastic behaviour of NREL 5MW turbine and one of the wind turbines from the Lillgrund wind park. The estimated power production using both aeroelastic coupled with DIWA turbulence boxes and standalone DIWA (without aeroelastic) are in good agreement with the literature data. The trends of fatigue loads are predicted well, with a few exceptions.

1. Introduction

Wind power is identified by the Intergovernmental Panel on Climate Change (IPCC) as one of the most promising renewable energy technologies for competing on cost with existing energy sources. Wind energy is the fastest growing source of renewable energy, as the global installed capacity has more than doubled between 2011 and 2016, reaching 467 GW[1], and it is expected to double in next five years[2]. Future deployment of wind power is almost at the point where governmental incentives are not needed anymore. In some parts of the world, wind energy is already competitive. Still, a number of economic and operational factors accompanied by regular maintenance on the smaller size of wind farms are some of the bottlenecks of further development of wind parks. One of the solutions is to develop wind farms with large arrays of wind turbines. A major problem while installing wind turbines in large arrays is an increased wake penalty that arises when a wind turbine operates in the wakes of neighboring upwind turbines. Wake from wind turbines in a wind farm leads to a reduction of the energy production. The wake also increases dynamic loading due to increase in the turbulence and meandering of the wakes. Understanding the wake patterns in a wind farm is identified as an important factor while designing and operating a wind farm to reduce the cost of energy production [1]–[8].

[1] http://www.irena.org/-/media/Files/IRENA/Agency/Publication/2017/Jul/IRENA_Renewable_Energy_Statistics_2017.pdf

[2] http://publikationen.windindustrie-in-deutschland.de/kostensituationder-windenergie-an-land-in-deutschland-update/54882668

The wake is generally divided into two regions, i.e., the near wake and the far wake. The near wake is the area just behind the turbine rotor and extends approximately two to three rotor diameters downstream. The near wake region is dominated by intense turbulence and large pressure gradients. The flow in near wake region mainly depends on inflow conditions and on the turbine properties i.e. the number of blades, the shape of turbine blades, the control system and both rotor and hub diameter. The far wake region extends downwind of the near wake and both turbulence mixing and mutual interaction of the wakes play an important role in the far wake. [9]. The wake flow pattern in the far wake region influences the aeroelastic behavior and power output of the downstream wind turbines

The wake behind the turbine is not stationary and it meanders mainly in transverse and lateral directions. The meandering of the wake significantly increases the fatigue loads on the wind turbines. An improved understanding of wake deficits, turbulence and dynamic movement of wakes is an essential key towards wind farm optimization studies[4], [10]–[16]. There are several approaches to model the wake and wake meandering. Models based on Computational Fluid Dynamics (CFD) are computationaly demanding but provide detailed description of the flows. On the other hand engineering models are much faster than CFD but often simplified to the extent where they cannot model basic physical phenomena such as partial wake operation or dynamic movements of the wakes [17], [18]. The DWM model developed by Madsen et. al. [17] is an alternative that includes some of the basic physical phenomena of meandering and DWM model is a relatively fast.

The characteristics and the underlying mechanisms behind the wake meandering are still not fully understood. Two hypothesizes of wake meandering have been proposed. The first hypothesis proposed by Madsen et. al. [17] state that the large-scale turbulent eddies contained in the atmospheric flows are responsible for wake meandering. Second hypothesis state that the meandering is due to the intrinsic instabilities of the wake characterized by a periodic vortex shedding within the wake [19], [20]. In the first hypothesize, it is assumed that small-scale eddies, smaller than the rotor diameter, are mainly responsible for turbulence mixing. Whereas the large-scale eddies, larger than the rotor diameter, are responsible for the meandering of the wakes [21], [22]. Both Bingöl et al. [23] and Trujillo et. al. [24] verified the first hypothesis by performing a couple of field measurements. Bingöl et al. [23] used one dimensional and Trujillo et. al. [24] used two dimensional nacelle-mounted lidar field measurements to verify the hypothesis. According to Bingöl et al. [23] for a sufficiently highly loaded rotor, the rotor will act as a solid disc where the flow separates at the disc's edge and vortex shedding will start. However, substantially low-frequency tower reaction forces due to vortex shedding have never been reported from full-scale load measurements. This argument from Bingöl et al. [23] indicates that the second hypothesis is not possible.

On the other hand, the Strouhal number[3] of the meandering is reported to be 0.1–0.3 [25]–[27] which is in favour of the second hypothesis. The Strouhal number of wake for a circular disc is around 0.12, which according to Medici [28] is close to the Strouhal number of a wind turbine operating at high tip-speed ratios. According to Okulov et al. [25], the first hypothesis assuming meandering a low frequency movements of the wake due to large scale fluctuations of the incomming atmospheric turbulence is not possible because large scale atmospheric fluctuations do not apear in wind or water tunnel experiments.

A study performed by Coudou et al. [20] indicates that meandering is a combination of both mechanisms. Although the value of Strouhal number obtained from wake data is in favor of the second hypothesis, meandering does not appear when integral length scales are smaller than the rotor diameter. According to Coudou et al. [20], the wake-meandering phenomenon seems to be caused by the amplification of the intrinsic instabilities of the wake by large-scale turbulent eddies contained in the atmospheric boundary layer [20].

[3] The Strouhal number ($\mathrm{St} = {}^{fD}\!/_{U}$) is a dimensionless number describing oscillating flow mechanisms. Where f is the frequency of vortex shedding, D is the diameter of the wind turbine and U is the flow velocity.

Most of the design codes are based on the first hypothesis due to ease in implementation. The other approach of meandering based on vortex shedding is complicated to implement in design codes, probably we need detailed LES simulations or experiments to estimate the meandering pattern.

The DWM model developed by Risø/DTU [17], [18], [21] estimates wake expansion and dynamic meandering of the wakes with sufficient accuracy while maintaining an acceptably low computational cost. In the present study, an approach based on the first hypothesis is presented and DWM model developed by Risø/DTU [17], [18], [21] is implemented in commercial code SIMA developed by SINTEF. The new program is referred as "Disturbed Inflow Wind Analyzer" (DIWA). A benchmarking study of SIMA-DIWA with literature data [17], FastFarm and SOWFA data [29] are presented and discussed. Finally, the verified model has been applied to understand the effect of wake meandering on the aeroelastic behaviour of a turbine placed in the Lillgrund wind park. DIWA model is also employed to understand the aeroelastic behaviour of a park consisting of two NREL 5MW wind turbine in a row.

2. Methodology

The DIWA module mainly consists of three major submodels. 1) submodels for calculating near wake, and far wake deficits in the meandering frame of reference, 2) a submodel for meandering center calculation, and 3) a submodel of small-scale wake-added turbulence calculation. The magnitude of the wake-added turbulence is based on the local wake deficit depth and the radial gradient of the wake deficit in the meandering frame of reference (MFoR). The major outputs of DIWA are power, thrust, meandering center positions, total turbulence, and average velocity of the turbines. In addition to this, turbulence boxes consisting of the ambient, added wake and meandering turbulences are written in both Mann and TurbSim format. These boxes have been used for aeroelastic simulations of the wind turbine. A brief description of DIWA implementation is presented in the following sections.

2.1. Induction Profile

The induced velocity caused by the incoming wind and the rotor rotation is computed based on the (Blade Element Momentum) BEM theory. This theory combines momentum theory and blade element theory. The general principle is that forces acting on the airfoil, based on empirical lift and drag coefficients, are balanced with the change in momentum of the air flowing through the rotor disk.

The balance of airfoil forces with the change in momentum of the air is the basic step in the calculation. In the implemented calculation, the dynamic wake method is used. Thus, the moment equations are solved once at each time step; i.e. no iterations. Each wind turbine blade is divided into blade elements. For each blade element, aerodynamic airfoil coefficients (lift, drag and moment) are defined as a function of the angle of attack and Reynolds number. These aerodynamic coefficients are specific for the type of airfoil used.

The induced velocities at the blade elements are computed assuming uniform and time-invariant wind flow that acts on a rigid-bladed rotor that rotates with constant speed. All blades are assumed to have the same constant pitch angle. The tower influence (shadow) effect is disregarded. The applied time stepping procedure terminates when the solution has converged so that the computed induced velocity is stable. The induction factor at each blade element is then taken as the resulting wind velocity in wind direction normalized by the undisturbed wind velocity in the longitudinal wind direction. The induction profile is defined as the set of induction factors at a normalized radial position along one blade from root to tip.

2.2. Start Deficit: Near Wake Deficit

A model for calculating the inlet velocity profile or start deficits at the rotor plane was proposed by Madsen et. al. [17]. The velocity profiles in the near wake region are estimated from the azimuthally and time-averaged axial induction profile as a function of radial position. The following equations are solved in the near wake region.

$$r_{w,i+1} = \sqrt{\frac{(1-a_i)}{(1-2a_i)}\left(r_{t,i+1}^2 - r_{t,i}^2\right) + r_{w,i}^2} \tag{1}$$

$$U_w\left(\left(r_{w,i+1} + r_{w,i+1}\right)/2\right) = U_0\left((1-2a_i)\right) \tag{2}$$

Where, r_w is the radius of i^{th} the stream tube at the end of the near wake regime, which varies with the induction profile, free stream velocity, and rotor radial dimensions. U_w is the radial velocity at r_w. The number of streamlines are equal to the number of elements used for calculating the induction profile in BEM.

2.3. *Near-Wake length model (NWL)*

Near-wake length is referred to the extent of the near wake region from the rotor plane. Ainslie proposed a fixed near wake length of 2 rotor diameters (D). However, the offshore ambient turbulence (6-8%) is typically much less than on land turbulence (10% – 12%). The lower turbulence intensity leads to a slower wake recovery and therefore to a longer near wake [30]. The NWL model has therefore been extended by implementing two different approaches. The first approach was proposed by Vermuelen [31] and the second approach was proposed by Sørensen [32]

2.3.1. Vermeulen NWL approach *[31]*

The near wake length (NWL) is a function of wake growth rate dr/dx, rotor radius, and thrust coefficient. The NWL is defined as

$$\left(\frac{l}{R}\right)_{near-wake} = \sqrt{\frac{m+1}{2}}\frac{\left(1-\sqrt{0.134+0.124m}\right)\sqrt{0.214+0.144m}}{\left(1-\sqrt{0.214+0.144m}\right)\sqrt{0.134+0.124m}}\left(\frac{dr}{dx}\right)^{-1} \tag{3}$$

Where, m is defined as $m = 1/\sqrt{1-C_T}$ The wake growth rate (dr/dx) constitutes of three different turbulence components i.e. ambient turbulence, rotor-generated turbulence and shear-generated turbulence.

$$\frac{dr}{dx} = \sqrt{\left(\frac{dr}{dx}\right)_\alpha^2 + \left(\frac{dr}{dx}\right)_m^2 + \left(\frac{dr}{dx}\right)_\lambda^2} \tag{4}$$

Where,

$\left(\frac{dr}{dx}\right)_\alpha = 2.5I_0 + 0.005$ is the contribution due to the ambient turbulence.

$\left(\frac{dr}{dx}\right)_m = \frac{(1m)\sqrt{1.49+m}}{(1+m)9.76}$ is the contribution due to the shear-generated turbulence.

$\left(\frac{dr}{dx}\right)_\lambda = 0.012N_b\lambda$ is the contribution due to the rotor-generated turbulence according to the number of blades N_b and the tip speed ratio λ. For offshore conditions, a slower wake recovery leads to a longer near wake and therefore the NWL will be either equal to or more than 2 times turbine rotor diameter with this model.

2.3.2. Sørensen approach [32]

Sørensen et al. [16] developed a model for Near-Wake Length Based on Stability Analysis. Large-eddy simulations (LES) using the actuator line (ACL) method was used by them to determine the NWL. The NWL was based on the instability onset of the trailing tip vortices shed from the turbine blades.

$$\left(\frac{l}{R}\right)_{near-wake} = \left(\frac{6.22}{N_b \lambda C_T} + 3\right)\log\left(\frac{T_i}{3}\right) \tag{5}$$

Where, C_T is the average thrust coefficient of the blade, T_i is the turbulence intensity. The model depends on the turbulence intensity and blade properties. The NWL will be either equal to or more than two times turbine rotor diameter.

2.4. Far Wake Region

The thin shear layer (TSL) approximation of the rotationally symmetric Navier-Stokes equations is employed [33]. Ainslie [33] assumed that in the far wake region, effects due to the pressure changes are insignificant and turbulent diffusion plays a significant role. The far wake region is modelled by the following axial momentum and the continuity equations

$$U\frac{\partial U}{\partial x} + V_r\frac{\partial U}{\partial r} = \frac{\nu_t}{r}\frac{\partial}{\partial r}\left(r\frac{\partial U}{\partial r}\right) \tag{6}$$

$$\frac{\partial U}{\partial x} + \frac{1}{r}\frac{\partial}{\partial r}\left(rV_r\right) = 0 \tag{7}$$

Where U denotes the axial velocity component, V_r is the radial velocity component, r is radial coordinates, ν_t is eddy viscosity.

Numerical methods are employed to solve momentum and continuity equations. The accuracy of the solution depends on the number of mesh points and the selected discretized scheme. In DIWA, two discretization schemes, 1) Central differencing and 2) Crank Nicolson are implemented for discretizing of TSL equations. The eddy viscosity (ν_t) is modelled using the following algebraic equation

$$\nu_t = F_2 k_2\left(\frac{b}{R}\right)\left(U_0 - U_{def,min}\right) + F_1 k_1 I_{amb} \tag{8}$$

Where $U_{def,min}$ is the minimum velocity at a given downstream location, and F_1 F_2 are filter function used for controlling the eddy viscosity. k_1 is the ambient eddy viscosity parameter, and k_2 is wake deficit eddy viscosity parameter. It has been assumed earlier that the effect of turbulence mixing on the wake expansion in the near wake region is insignificant. However, it has been observed from the previous studies [17] that the turbulent mixing also takes place in the near wake region, but the magnitude of the turbulent mixing is not very high and it varies linearly from the rotor plane to the NWL. In the near wake region, filter function F_1 is introduced to account for the turbulent mixing. The F_1 filter function varies linearly from 0 to 1 over the NWL. The filter function F_2 accounts for the turbulence generated by the wake deficits. In DIWA, F_1 and F_2 filter function from Madsen et. al. [17], Larsen et. al. [21] and Keck et. al. [18] are introduced. F_1 filter developed by Madsen et. al. [17] gave too low recovery of the velocity deficit at low turbulence intensities. This shortcoming was overcome by a non-linear coupling function F_{amb} and a modified filter function F_1 of the eddy viscosity to ambient turbulence intensity was introduced by Larsen et. al. [21].

$$\nu_t = F_2 k_2\left(\frac{b}{R}\right)\left(U_0 - U_{def,min}\right) + F_1 F_{amb} k_1 I_{amb} \tag{9}$$

Keck et al. [3] calibrated F_2 filter function with LES data at few selected axial distances and he proposed following filter function

$$F_1 = \begin{cases} x / NWL & x < NWL \\ 1 & x > NWL \end{cases} \quad (10)$$

$$F_2 = \begin{cases} 0.035 & x <= NWL \\ 1 - 0.965e^{-0.35(x-NWL)} & x > NWL \end{cases} \quad (11)$$

Where x refers to the downstream position in rotor diameters from the wake emitting turbine.

2.5. Modelling of meandering

The meandering model implemented in DIWA is based on the approach proposed by Larsen et al. [21]. In the meandering implementation, it is assumed that each wake deficits from the wind turbines acts as a passive tracer and movements of the tracers are mainly controlled by the large-scale ambient turbulence fluctuation, which in DIWA can be calculated either using Mann Turbulence generator or TurbSim. In the DIWA implementation, the tracer movement in the wind direction due to the longitudinal velocity fluctuation is assumed to be negligible. According to Larsen et al. [21], the longitudinal turbulence will only affect the time scales of the passive tracer/deficit wake centre and these time scale effects are of secondary importance.

In the present implementation, the following approach [21] has been implemented. It is assumed that n wakes are released from the wake-emitting turbines with a time interval Δt. Instantaneous release time t_i of the i^{th} wake is given by $t_i = t_0 + i\Delta t$;

The initial position of the wake centre of the i^{th} wake is assumed to be at the hub of the wind turbine and transverse position of the hub is assumed to be zero.

$$y_c = 0 \quad (12)$$

$$z_c(t_i) = H_{hub}; \quad (13)$$

Where x_c , y_c and z_c are the axial, lateral, and transverse coordinate of the wake centre. The current wake centre position $(x_{c+1}, y_{c+1}, z_{c+1})$ of the deficit is estimated from the previous wake centre position (x_c, y_c, z_c) using the following relation

$$x_{c+1} = x_c + U\Delta t \quad (14)$$

$$y_{c+1} = y_c + v_f\left(U[T - t_i], y_c, z_c\right)\Delta t \quad (15)$$

$$z_{c+1} = z_c + w_f\left(U[T - t_i], y_c, z_c\right)\Delta t \quad (16)$$

Where U is the free-stream velocity, v_f and w_f are filtered lateral and transverse velocity components. A low pass filter is employed to obtain the filtered velocities (v_f and w_f). The turbulence characteristics smaller than the instantaneous wake width are filtered out.

3. Benchmarking

3.1. Benchmarking: Verifications and validation

Verification and validation are critically important for establishing the credibility and acceptance of SIMA-DIWA for wind farm simulations. The definition of verification and validation are defined by the AIAA (1998) guide as [34].

- Verification refers to the accurate implementation of the previous models and the solution of the models [35].
- Validation refers to an accurate representation of the new methods and new approach compared with the previous well-established data [35].

The SIMA-DIWA model is benchmarked with Literature data [17], FastFarm and SOWFA data [29], [36]. The benchmarking includes verification of quasi-steady wake deficits, far wake deficits, and power and thrust prediction. The quasi-steady wake deficit (near wake profiles) at 2D downstream was

verified with the results from the uniformly loaded actuator disk. The data for verification studies were taken from previous DWM studies carried out by Madsen et al. [17]. The axial velocity profiles for the DIWA and DWM data [17] are shown in Figure 1. These DWM data were generated by HAWC2 by Madsen et al. [17] The axial velocities compare well with the DWM data. The first validation (see Figure 1) was performed to verify quasi-steady wake deficits and second verification (see Figure 2) was carried out to verify far wake deficit profiles. The far wake model was verified with literature data at 8 m/s and at downstream stream distances of 3D, 6D, and 10D and for ambient turbulence levels of 5%, 10%, and 15%. In the present study, the results only at 5% turbulence intensity are presented. Following parameters were used in DIWA: k_2=0.008, k_1=0.07, km_1=0.6, and km_2=0.35 and the filter functions F_1 and F_2 as proposed by Madsen et al. [17]. The mean velocity and total turbulence intensities at various downstream distance i.e. 3D, 6D, and 10D for turbulence intensity of 5% are shown in Figure 2. The total turbulence includes a contribution from ambient, meandering and added wake. The axial velocity profiles compare well with the literature data, but the total turbulence is underpredicted at a distance 10 diameter downstream. This could be due to underprediction in a meandering pattern. In all the figures "X" refers to the axial distance from the wake emitting turbine and r is the radial position from the axis of the turbine.

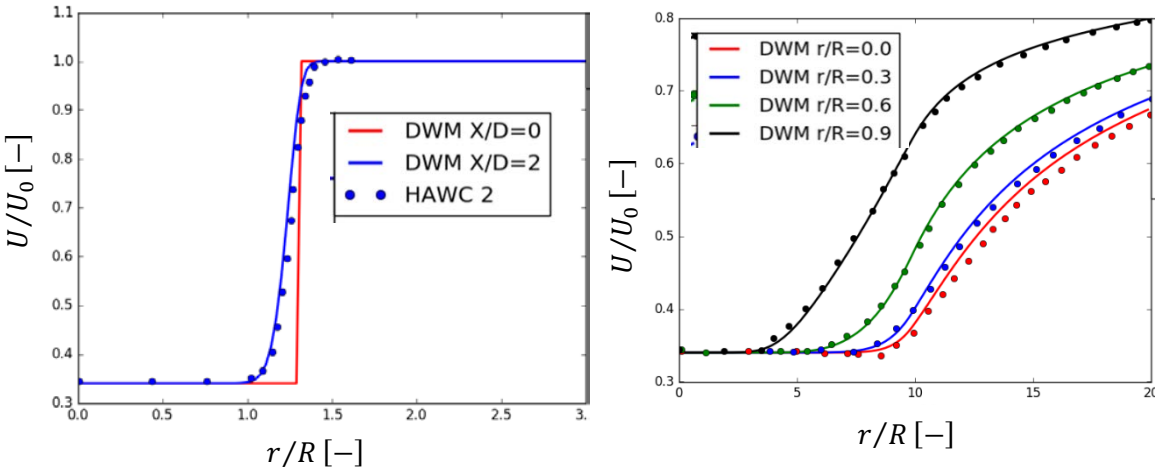

Figure 1 Radial profile of axial velocity (left) and axial profiles of velocity (right) for constant turbine loading. *(Solid lines are from DIWA and bullet points are from HAWC 2)*

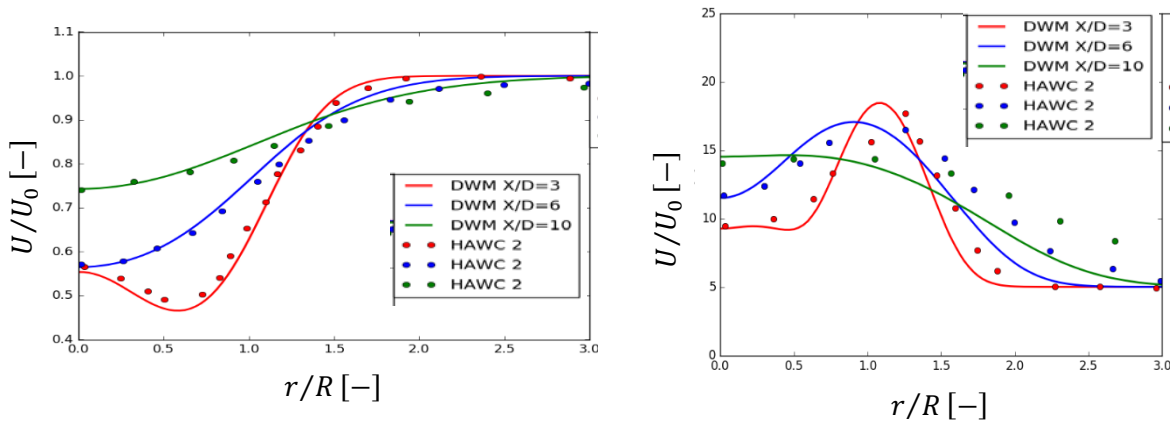

Figure 2 Radial profile of Velocity deficits and total turbulence intensity of deficits at constant turbine loading *(Solid lines are from DIWA and bullet points are from HAWC 2)*

3.2. Benchmarking with SOWFA and FastFarm

DIWA simulations of a park consisting of three NREL 5MW wind turbines in a row were performed. The distance among turbines was 8D. The mean velocity at the inlet was set equal to 8 m/s and two DIWA simulations at 6% and 10% of turbulence intensities were performed. The wake deficits obtained from DIWA is compared with FastFarm and SOWFA results [29]. In DIWA calculations, the ambient eddy viscosity parameter k_1 was made a function of turbulence intensities. Temporal and azimuthal averaged radial profiles of the axial wake deficits in the meandering frame of reference at 2D, 4D and 6D downstream of the second wind turbine at 6% and 10% of turbulence intensities are shown in Figure 3 and Figure 4, respectively. The negative wake deficits indicate that the velocity behind the turbine is lower than the free stream wind velocity. The wake deficit behind the wind turbine follows a Gaussian shape and strongest wake deficit is observed near to the axis of the turbines. Overall the wake deficits profiles obtained from DIWA agree reasonably well with the SOWFA and FastFarm. However, a discrepancy in the wake deficits profile at 2D is due to near wake phenomena which is difficult to predict accurately. Further downstream results from the DIWA compares well with the SOWFA and FastFarm (FF) predictions.

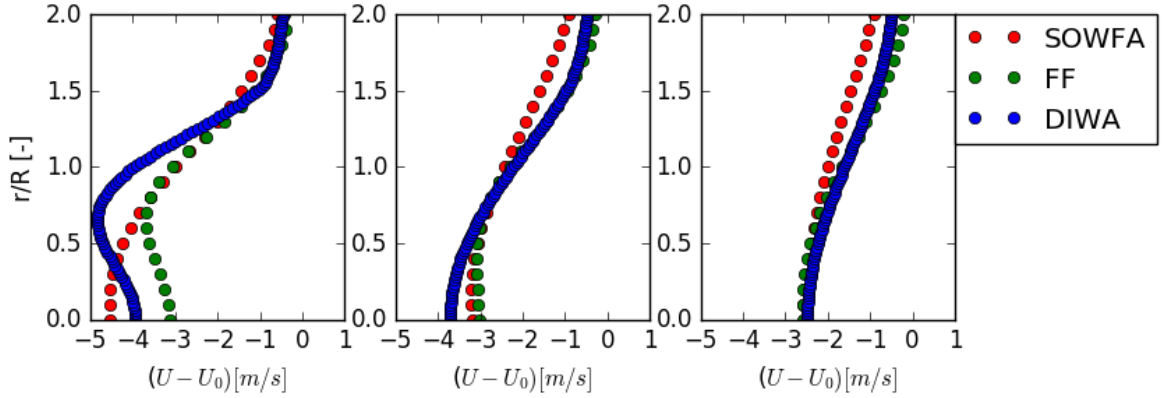

Figure 3 Radial profiles of axial velocity deficits at 2D, 4D and 6D downstream of the second wind turbine for the wind velocity of 8m/s and turbulence intensity of 6%

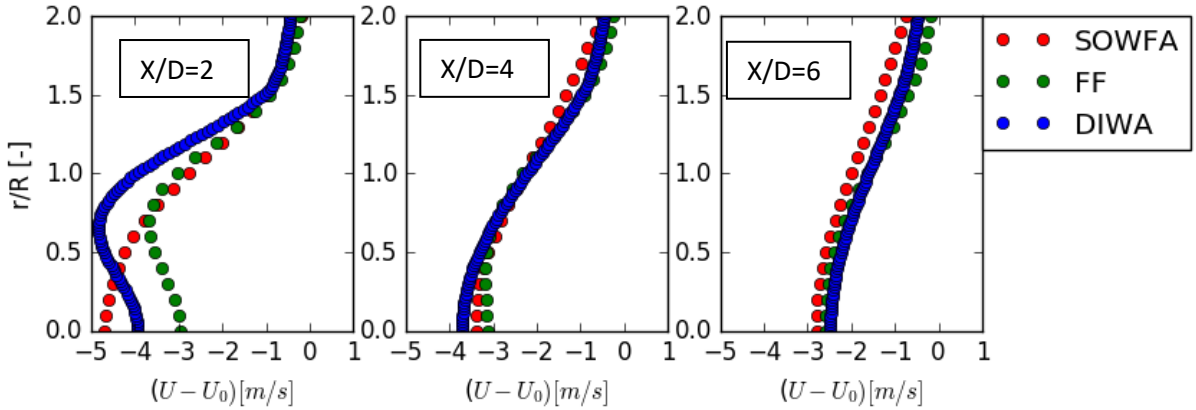

Figure 4 Radial profiles of axial velocity deficits at 2D, 4D and 6D downstream of the second wind the wind turbine for a wind velocity of 8m/s and turbulence intensity of 10%

4. Standalone DIWA power and thrust tool

The power estimation of the standalone DIWA is based on the time and area averaged mean flow field at the rotor. Here, standalone DIWA refers to the simulations without aeroelastic coupling (without Riflex). In the standalone DIWA, the induction profiles are estimated using inbuilt blade element method and it does not require any coupling with aeroelastic code.

The power is a nonlinear function of the wind speed (cubic in the wind speed). In DIWA, power is calculated in two steps; in step-1, the average speed at the target turbine is calculated by area and time averaging. In the second step, the instantaneous power is calculated from the turbine performance table using the average speed from step-1. The turbine performance table mainly consists of the power and thrust profiles as a function of wind speed. The performance table is a turbine property and it is normally provided by wind turbine suppliers.

Verification studies of standalone DIWA are presented and discussed. Two and three wind turbines of the Lillgrund wind farm at 4.3D turbine spacing (see Figure 5) [37], [38] was used for verification studies. The ambient wind speed and turbulence intensity were set to 8 m/s and 7% respectively. Figure 6 shows the normalized power production as a function of wind direction for a single-wake scenario (see Figure 6 (a)) and a double wake scenario (see Figure 6 (b)) respectively. Overall, DIWA normalized power prediction compares well with the field data. However, in the case of multiple wake conditions (i.e. double wake scenario), the DIWA underpredicts in full wake condition

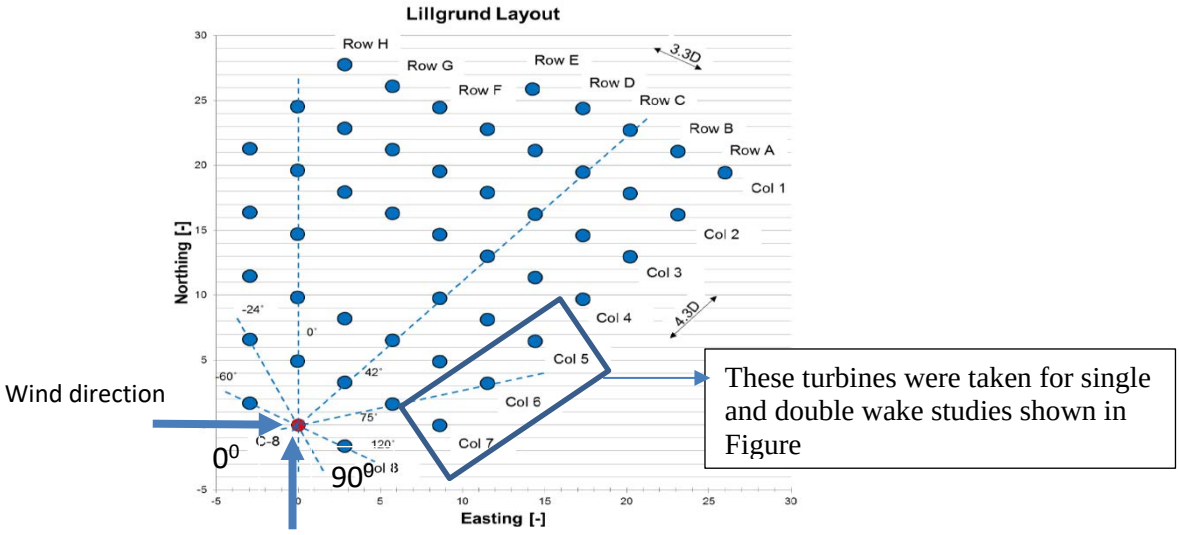

Figure 5: The Layout of the Lillgrund wind farm and location of WT C08 turbine. Distances are non-dimensioned with the rotor diameter (**please note that the wind direction does not standard convection**: 0 degrees is from the north and 90 degrees is from the east)

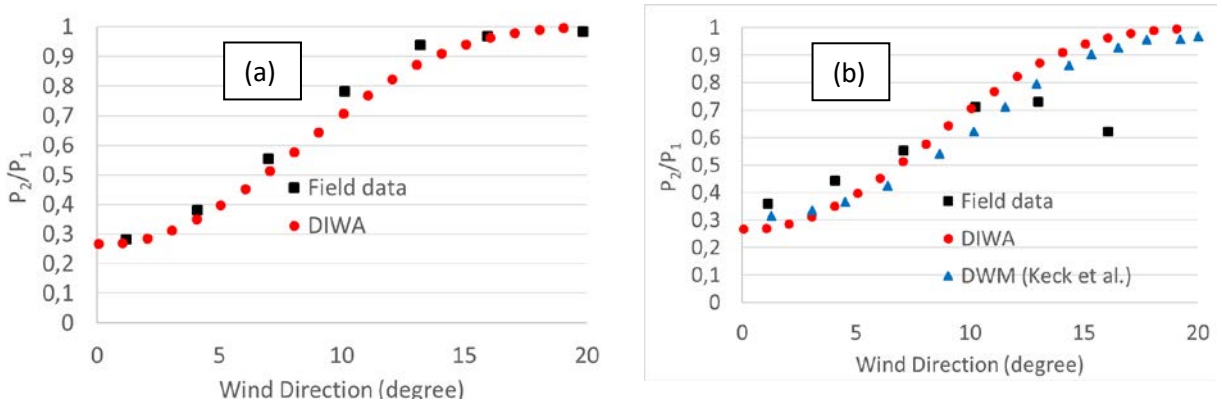

Figure 6 Normalized power production as a function of wind direction for a single-wake scenario (a) and double wake scenario

Just to clarify, the standalone DIWA simulations only include a single row consisting of three turbines in the double-wake situation, whereas the field data includes the whole wind farm with 48 wind turbines. Therefore, the field data shows non-linear behaviour above wind direction of 12 degree. Standalone DIWA was used for the power calculation of C08 wind turbine of the Lillgrund wind farm (see Figure 7). The wind direction coordinate system used in DIWA is shown in Figure 5. DIWA model input parameters were set as a default (k_1 = 0.1; k_2 = 0.008; wake deficit operator = max). The ambient velocity was set to 9 m/s and turbulence intensity was set to 6%. Around 72 simulations covering the 0–360 degree polar with a resolution of 5 degrees for the whole park were performed. Power predicted using DIWA and HAWC2 in various wind direction is shown in Figure 7.

The DIWA results are in a reasonable agreement with HAWC2. The best agreement between DIWA and the HAWC2 is observed in the wind directions from 0 to 180 degrees. DIWA, however, underpredicts the power for wind direction from 180 to 300 degrees. A reason for this could be the wake behavior at the C08 wind turbine from the neighboring turbines. The C08 wind turbine is subjected to multiple deficits in the wind direction from 180 to 300 degree. The DIWA model seems to be underpredicting the power under multiple wake scenario. Similar behavior has been observed in the double wake scenario in the previous section (see Figure 6). This could be due to a different approach of power calculation used in DIWA compare to HWAC2. DIWA standalone averages velocity at the wind turbine and then power is estimated from the power performance table using the average velocities. HWAC2 calculations are based on full aeroelastic simulations.

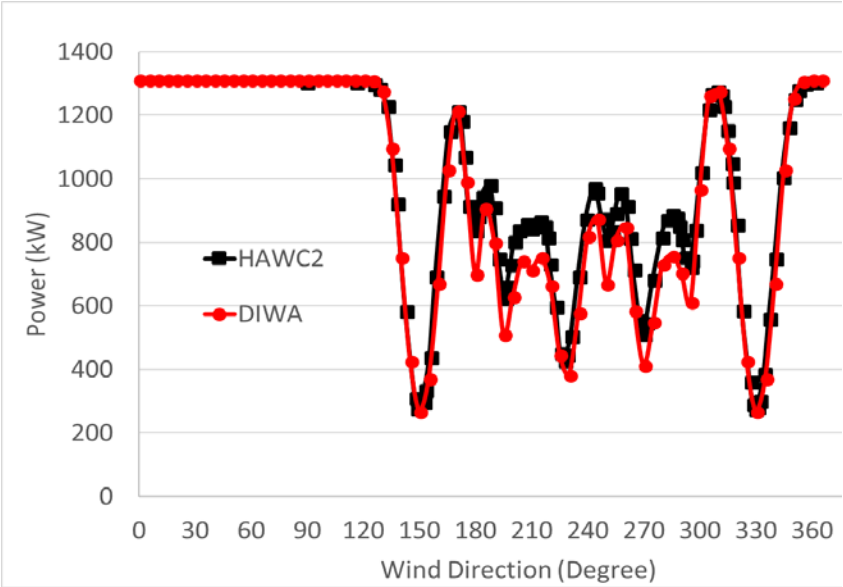

Figure 7: Power of WT C08 turbine in the Lillgrund wind farm compared with data [17] at wind direction from 0 to 360 degree with an interval of 5 degrees.

DIWA was also used for power calculation of the entire Lillgrund wind farm (see Figure 8). In DIWA calculations, the model input parameters were set as a default (k_1 = 0.1; k_2 = 0.008; wake deficit operator = max). The ambient velocity was set to 9 m/s and turbulence intensity was set to 6%. A script was used for performing many park simulations consisting of all wind directions. Simulations covering the 0–360 degree polar with a resolution of 5 degrees for the whole park were performed. The total power of the wind farm was written as a function of wind direction. In wind farm verification and validation studies, the wake deficits profiles and turbulent kinetic energy are very important parameters as they are directly related to the annual energy production and loading [35], [38]. However, these variables are difficult to find from the literature and only the power data and park efficiencies are mainly available from the literature. In this study, DIWA park efficiency at various wind direction have been

compared with the field data [35]. The park efficiency η is defined as ($\eta = \frac{P_{wake}}{P_{free}}$). Where, P_{wake} and P_{free} are the power production of a turbine in waked and free wind conditions respectively[35]. The effect of the wind direction on park efficiencies for the whole wind farm is shown in Figure 8. An overall effect of wind direction on the park efficiency is predicted well with DIWA. However, DIWA tends to overpredict the power for wind direction less than 150 degrees. For wind direction above 150 degrees, the power prediction is in good agreement with data. The wake efficiency is largely underestimated in full-wake conditions or multiple wake scenario. It is to be noted that the field data are averaged for wind direction uncertainties but the DIWA are without wind direction averaging.

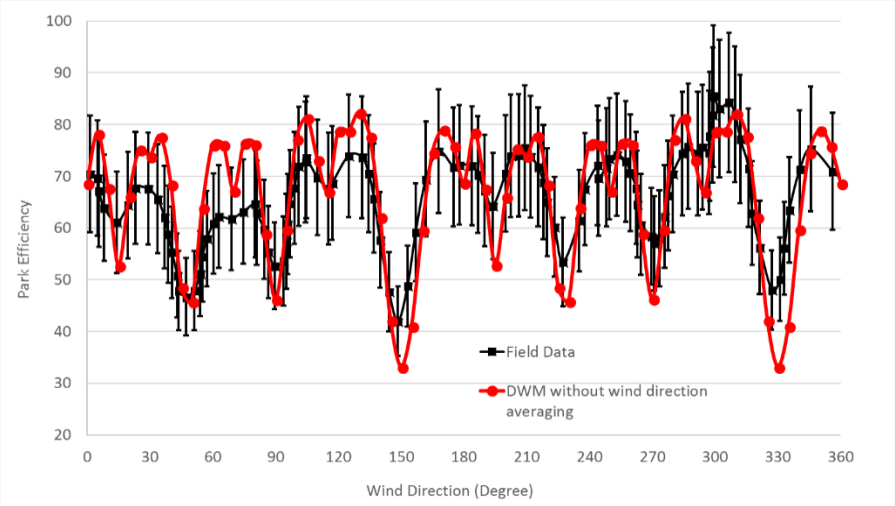

Figure 8: Total park efficiency of Lillgrund wind farm compared with field data at wind direction from 0 to 360 degrees with an interval of 5 degrees.

5. Aeroelastic Simulation

5.1. Aeroelastic studies of NREL 5MW turbine

A verification study that compares the power and thrust force output of DIWA and aeroelastic software Riflex is presented and discussed. A simple park layout was assumed, using only two turbines in the row, the upstream turbine creates a wake for the downstream turbine. Six different spacings were investigated, representing from approximately 3 to 8 rotor diameters. Each DIWA simulation needs a set of three ambient turbulence boxes; The meandering turbulence box (coarse grid), the added wake turbulence box (fine grid) and the ambient turbulence box. The turbulence was generated by the Mann Turbulence Generator. A comparison of the power obtained using DIWA and Riflex for both flexible and rigid induction profile is shown in Figure 9. 50% difference between DIWA and aeroelastic calculation for 6 m/s wind with 3D distance, reduced to 30% when assuming a flexible induction profile. However, 3D distance is a very unrealistic turbine spacing for modern wind farms. For a distance of 6-8D the difference between DIWA and aeroelastic was less than 20%

5.2. Aeroelastic simulations of C08 turbine of Lillgrund wind park

Aeroelastic simulations of the C08 wind turbine placed in the Lillgrund wind park are performed in SIMA using aeroelastic code SIMA-Riflex, which is a tailor-made tool for static and dynamic analysis of slender marine structures. Riflex can be used in nonlinear time-domain simulation, combined wave, wind and current loads, wind generated forces on the turbine rotor and and tower. The major inputs for Riflex are turbulent wind boxes, turbine and blade properties, operational wind condition.

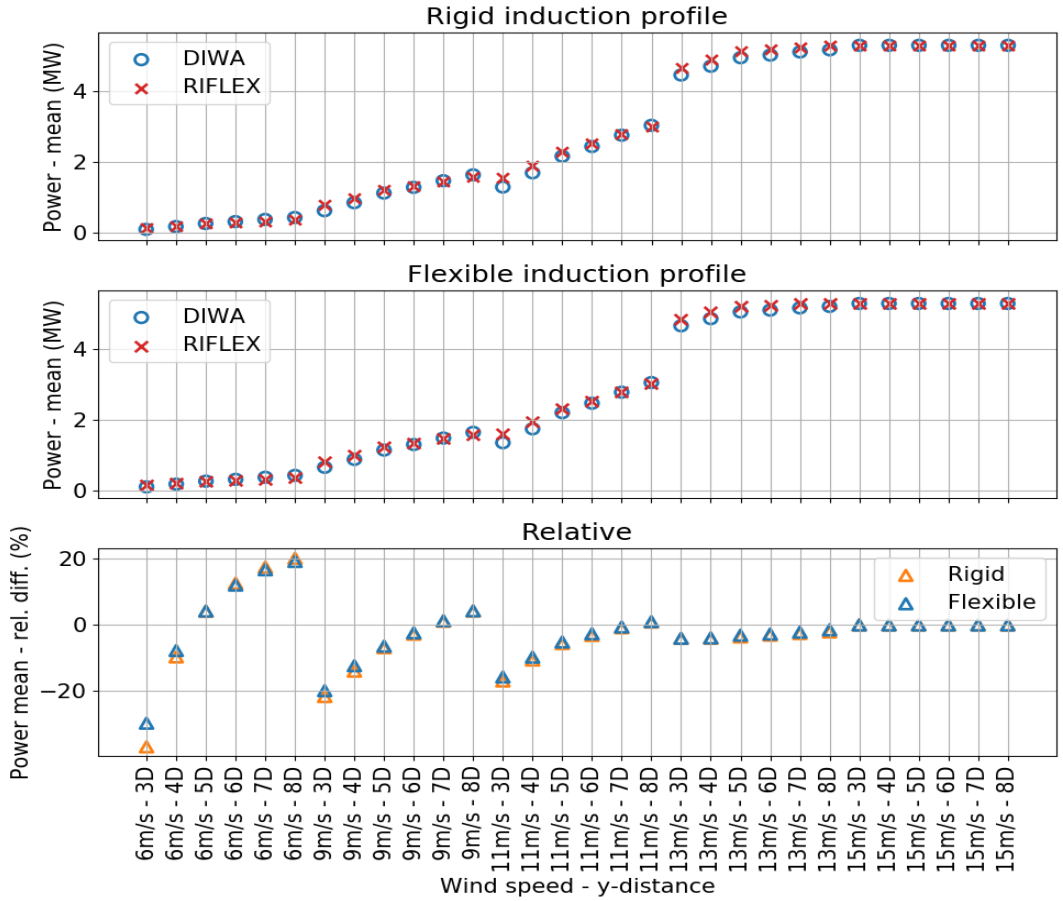

Figure 9: Mean power for DIWA and for the aeroelastic model, for rigid (top) and flexible (middle) induction profiles.

The turbulence intensity at Lillgrund for lower wind speeds (6 m/s-14 m/s) is 5.8%. In this study, the Mann turbulence generator was used to generate the ambient wind field, the coarse wind field used as input to the meandering and the fine grid used as input to the added turbulence. Based on the three input wind fields, the layout of the windfarm and the wind direction, the DWM tool will generate a wind box to be applied to the target turbine C08.

Different random seeds are used to generate six ambient wind fields, six wind fields with a coarse grid, and six wind fields with finer grids. These are used as input to the DIWA, that returns six wind fields for each wind direction considered. The results are presented in this section. Figure 5shows the layout of Lillgrund windfarm as modelled in DIWA with some of the important wind directions marked. These wind directions will be used when presenting the results later. The minimum distance from the target turbine to source turbines, 3.3 D, is found at 330 deg and 150 deg.

The turbine used in Lillgrund wind park is based on the modelled wind turbine proposed by Churchfield et al. [39], [40]. The rotor and hub diameter of the turbine is 93 m and 3 m respectively. The weight of the rotor and nacelle is around 60 ton and 83 ton respectively. The cut-in, cut-out and rated speed of the wind turbine are 3, 25 and 10.9 m/s respectively. The rated power of the turbine is 2.3 MW. Blades are modelled as stiff, and the tower eigenfrequency is placed between the 1P and 3P region. An overview of the first five eigenfrequencies is given in Table 1. The blades are modelled stiff, and the modes are therefore all tower modes.

Table 1: First five eigenfrequencies of the wind turbine structure.

Mode No	Mode Name	Frequency [Hz]	Period [s]
1	Side-to-side	0.33	3.06
2	Fore-aft	0.33	3.06
3	Torsion	1.77	0.56
4	2nd side to side	2.23	0.45
5	2nd fore-aft	2.42	0.41

6. Power production using Aeroelastic code Riflex

Six simulations are performed for each wind direction. These are represented with blue markers in the results figures. The red markers are the mean values. It was chosen to consider the wind directions from 90 degrees to 360 degrees. The estimated power production based on the aeroelastic calculations is shown in Figure 10. The initial offset between random seeds in produced power originates from small offsets in mean wind speed in the turbulence box. Although the theoretical mean of a turbulence box is zero, small variations around zero is observed in the realizations. A similar study of the power production has previously been done in HAWC2, and these data are also included for comparison. The numerical models are not identical, and a perfect match is therefore not expected. The trends in the results are quite similar, with the peaks and the throughs at the same locations.

Damage equivalent load (DEL) calculated using SIMA-DIWA is compared with HAWC2 simulations [41] and shown in Figure 11. The DEL results do not show a good comparison, but this is likely to be due to the differences in the control system and in the aeroelastic models HAWC2 and SIMA-DIWA. However, one can see that the trends are similar. Two wind directions that show opposite trends compared to the HAWC2 data are at 210 and 250 degrees. The mean wind speed on the target turbines for these directions are similar and diverging trends could be due to rotational frequency resonance. In absence of proper input data (structural and control system), it is difficult to compare SIMA-DWM with the HAWC2 in more detail. Please not the 0.3D, 6D, 4.3D etc shows the distance from the turbine.

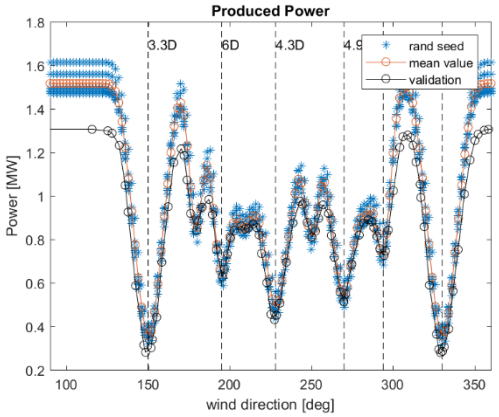

Figure 10: Estimated produced power from simulations. Blue indicates each random seed, red is the mean value and black is the benchmark values from HAWC2 (here 3.3D, 6D, etc represent distance between two turbines)

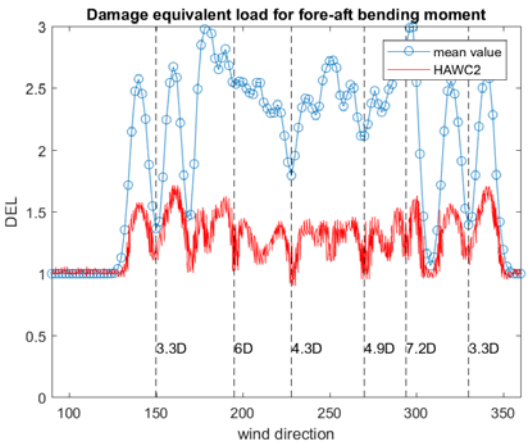

Figure 11: Damage equivalent load compared with HAWC2 simulations

7. Conclusions

Two hypothesizes for the wake meandering are identified based on the literature study. A first hypothesis state that the wake meandering is due to large-scale turbulent eddies contained in the atmospheric boundary layer. Second hypothesis state that the meandering is due to the intrinsic instabilities of the wake characterized by a periodic vortex shedding within the wake. However, most of the design codes are based on the first hypothesis. Dynamic meandering model based on the first meandering hypothesis has been implemented in SIMA software. The new implementation "SIMA-DIWA" is benchmarked against the literature data. The study indicates that the eddy viscosity model parameters and filter functions play important role in wake deficits. The estimated power production based on the aeroelastic coupled with DIWA turbulence boxes and standalone DIWA is in good agreement with the literature data. The trends of fatigue loads are predicted well, with a few exceptions.

For future studies, the ambient turbulence parameters as a function of turbulence intensity and axial distance will be developed. Furthermore, a dynamic eddy viscosity model will be proposed and tested to improve the predictions.

8. References

[1] J. N. Sørensen, W. Z. Shen, and X. Munduate, 'Analysis of wake states by a full-field actuator disc model', *Wind Energy*, vol. 1, no. 2, pp. 73–88, Dec. 1998.
[2] J. N. Sørensen and C. W. Kock, 'A model for unsteady rotor aerodynamics', *J. Wind Eng. Ind. Aerodyn.*, vol. 58, no. 3, pp. 259–275, Dec. 1995.
[3] I. Ammara, C. Leclerc, and C. Masson, 'A Viscous Three-Dimensional Differential/Actuator-Disk Method for the Aerodynamic Analysis of Wind Farms', *J. Sol. Energy Eng.*, vol. 124, no. 4, p. 345, 2002.
[4] J. N. Sørensen and W. Z. Shen, 'Numerical Modeling of Wind Turbine Wakes', *J. Fluids Eng.*, vol. 124, no. 2, p. 393, 2002.
[5] R. Gómez-Elvira, A. Crespo, E. Migoya, F. Manuel, and J. Hernández, 'Anisotropy of turbulence in wind turbine wakes', *J. Wind Eng. Ind. Aerodyn.*, vol. 93, no. 10, pp. 797–814, Oct. 2005.
[6] A Jimenez and A Crespo and E Migoya and J Garcia, 'Advances in large-eddy simulation of a wind turbine wake', *J. Phys. Conf. Ser.*, vol. 75, no. 1, p. 012041, 2007.
[7] A Jimenez and A Crespo and E Migoya and J Garcia, 'Large-eddy simulation of spectral coherence in a wind turbine wake', *Environ. Res. Lett.*, vol. 3, no. 1, p. 015004, 2008.
[8] A. El Kasmi and C. Masson, 'An extended model for turbulent flow through horizontal-axis wind turbines', *J. Wind Eng. Ind. Aerodyn.*, vol. 96, no. 1, pp. 103–122, Jan. 2008.
[9] L. J. Vermeer, J. N. Sørensen, and A. Crespo, 'Wind turbine wake aerodynamics', *Prog. Aerosp. Sci.*, vol. 39, no. 6–7, pp. 467–510, Aug. 2003.
[10] J. N. Sørensen, 'Aerodynamic Aspects of Wind Energy Conversion', *Annu. Rev. Fluid Mech.*, vol. 43, no. 1, pp. 427–448, Jan. 2011.
[11] R. J. Barthelmie *et al.*, 'Flow and wakes in large wind farms in complex terrain and offshore', 2008.
[12] R. J. Barthelmie *et al.*, 'Modelling and measurements of wakes in large wind farms', *J. Phys. Conf. Ser.*, vol. 75, p. 012049, Jul. 2007.
[13] R. J. Barthelmie *et al.*, 'Comparison of Wake Model Simulations with Offshore Wind Turbine Wake Profiles Measured by Sodar', *J. Atmospheric Ocean. Technol.*, vol. 23, no. 7, pp. 888–901, Jul. 2006.
[14] F. R. Menter, R. Langtry, and S. Völker, 'Transition Modelling for General Purpose CFD Codes', *Flow Turbul. Combust.*, vol. 77, no. 1–4, pp. 277–303, Oct. 2006.
[15] M. Potsdam and D. Mavriplis, 'Unstructured Mesh CFD Aerodynamic Analysis of the NREL Phase VI Rotor', in *47th AIAA Aerospace Sciences Meeting including The New Horizons Forum and Aerospace Exposition*, Orlando, Florida, 2009.
[16] Y.-T. Wu and F. Porté-Agel, 'Large-Eddy Simulation of Wind-Turbine Wakes: Evaluation of Turbine Parametrisations', *Bound.-Layer Meteorol.*, vol. 138, no. 3, pp. 345–366, Mar. 2011.

[17] H. A. Madsen, G. C. Larsen, T. J. Larsen, N. Troldborg, and R. Mikkelsen, 'Calibration and Validation of the Dynamic Wake Meandering Model for Implementation in an Aeroelastic Code', *J. Sol. Energy Eng.*, vol. 132, no. 4, p. 041014, 2010.
[18] R.-E. Keck, H. A. Madsen, G. C. Larsen, D. Veldkamp, J. J. Wedel-Heinen, and J. Forsberg, 'A consistent turbulence formulation for the dynamic wake meandering model in the atmospheric boundary layer', 2013.
[19] D. Medici and P. H. Alfredsson, 'Measurements on a wind turbine wake: 3D effects and bluff body vortex shedding', *Wind Energy*, vol. 9, no. 3, pp. 219–236, May 2006.
[20] N. Coudou, S. Buckingham, and J. van Beeck, 'Experimental study on the wind-turbine wake meandering inside a scale model wind farm placed in an atmospheric-boundary-layer wind tunnel', *J. Phys. Conf. Ser.*, vol. 854, p. 012008, May 2017.
[21] G. C. Larsen, H. A. Madsen, K. Thomsen, and T. J. Larsen, 'Wake meandering: a pragmatic approach', *Wind Energy*, vol. 11, no. 4, pp. 377–395, Jul. 2008.
[22] G. C. Larsen, H. A. Madsen, T. J. Larsen, and N. Troldborg, 'Wake modeling and simulation', *Risø Natl. Lab. Tech. Univ. Den. Rep. No Risø*, 2008.
[23] F. Bingöl, J. Mann, and G. C. Larsen, 'Light detection and ranging measurements of wake dynamics part I: one-dimensional scanning', *Wind Energy*, vol. 13, no. 1, pp. 51–61, Jan. 2010.
[24] J.-J. Trujillo, F. Bingöl, G. C. Larsen, J. Mann, and M. Kühn, 'Light detection and ranging measurements of wake dynamics. Part II: two-dimensional scanning', *Wind Energy*, vol. 14, no. 1, pp. 61–75, Jan. 2011.
[25] V. L. Okulov, I. V. Naumov, R. F. Mikkelsen, I. K. Kabardin, and J. N. Sørensen, 'A regular Strouhal number for large-scale instability in the far wake of a rotor', *J. Fluid Mech.*, vol. 747, pp. 369–380, May 2014.
[26] D. Medici and P. H. Alfredsson, 'Measurements behind model wind turbines: further evidence of wake meandering', *Wind Energy*, vol. 11, no. 2, pp. 211–217, Mar. 2008.
[27] L. P. Chamorro, C. Hill, S. Morton, C. Ellis, R. E. A. Arndt, and F. Sotiropoulos, 'On the interaction between a turbulent open channel flow and an axial-flow turbine', *J. Fluid Mech.*, vol. 716, pp. 658–670, Feb. 2013.
[28] D. Medici, 'Experimental Studies of Wind Turbine Wakes – Power Optimisation and Meandering', p. 181.
[29] J. Jonkman, P. Doubrawa, N. Hamilton, J. Annoni, and P. Fleming, 'Validation of FAST.Farm Against Large-Eddy Simulations', *J. Phys. Conf. Ser.*, vol. 1037, p. 062005, Jun. 2018.
[30] B. Lange, H.-P. Waldl, A. G. Guerrero, D. Heinemann, and R. J. Barthelmie, 'Modelling of Offshore Wind Turbine Wakes with the Wind Farm Program FLaP', *Wind Energy*, vol. 6, no. 1, pp. 87–104, Jan. 2003.
[31] P. E. J. Vermeulen, 'An experimental analysis of wind turbine wakes', in *3rd International Symposium on Wind Energy Systems*, 1980, pp. 431–450.
[32] Jens N Sørensen and Robert Mikkelsen and Sasan Sarmast and Stefan Ivanell and Dan Henningson, 'Determination of Wind Turbine Near-Wake Length Based on Stability Analysis', *J. Phys. Conf. Ser.*, vol. 524, no. 1, p. 012155, 2014.
[33] J. F. Ainslie, 'Calculating the flowfield in the wake of wind turbines', *J. Wind Eng. Ind. Aerodyn.*, vol. 27, no. 1–3, pp. 213–224, 1988.
[34] Computational Fluid Dynamics Committee, Ed., *Guide: Guide for the Verification and Validation of Computational Fluid Dynamics Simulations (AIAA G-077-1998(2002))*. Washington, DC: American Institute of Aeronautics and Astronautics, Inc., 1998.
[35] P. Moriarty *et al.*, 'IEA-Task 31 WAKEBENCH: Towards a protocol for wind farm flow model evaluation. Part 2: Wind farm wake models', *J. Phys. Conf. Ser.*, vol. 524, no. 1, p. 012185, 2014.
[36] P. Doubrawa, J. R. Annoni, and J. M. Jonkman, 'Optimization-Based Calibration of FAST. Farm Parameters against Large-Eddy Simulations', in *2018 Wind Energy Symposium*, 2018, p. 0512.
[37] M. Gaumond *et al.*, 'Benchmarking of wind turbine wake models in large offshore wind farms', p. 8.

[38] R.-E. Keck, 'Validation of the standalone implementation of the dynamic wake meandering model for power production: Validation of the standalone DWM model for power production', *Wind Energy*, vol. 18, no. 9, pp. 1579–1591, Sep. 2015.
[39] M. Churchfield *et al.*, 'A Large-Eddy Simulations of Wind-Plant Aerodynamics', in *50th AIAA Aerospace Sciences Meeting including the New Horizons Forum and Aerospace Exposition*, Nashville, Tennessee, 2012.
[40] M. J. Churchfield, S. Lee, J. Michalakes, and P. J. Moriarty, 'A numerical study of the effects of atmospheric and wake turbulence on wind turbine dynamics', *J. Turbul.*, vol. 13, p. N14, Jan. 2012.
[41] Helge, 'Wake effects above rated wind speed. An overlooked contributor to high loads in wind farms'.

Acknowledgments
The work was performed at SINTEF, Norway under a project funded by Equinor ASA, Norway. The authors gratefully acknowledge the financial support received from the Equinor ASA, Norway. The authors also want to thank Dr. Jason Jonkman and Dr. Nicholas Hamilton from NREL, for providing the SOWFA and FastFarm data.